Journal of Medical Robotics Research, Vol. X, No. X (2017) X–X

Improved temporal calibration of tracked ultrasound: an open-source solution

Eric M. Moult[a], Andras Lasso[b], Tamas Ungi[b], Csaba Pinter[b], Mattea Welch[c] , Gabor Fichtinger[b]

[a]*Department of Electrical Engineering and Computer Science, MIT, Cambridge, MA, USA*
[b]*School of Computing, Queen's University, Kingston, ON, Canada*
[c]*Department of Medical Biophysics, University of Toronto, Toronto, ON, Canada*
E-mail: gabor.fichtinger@queensu.ca

In tracked ultrasound systems, temporal misalignment between image and tracker data results in incorrect image pose. We present a fully automatic temporal calibration. We image a flat plate in water with a tracked probe undergoing periodic uniaxial freehand translation. Using robust line detection scheme, we compute temporal misalignment as difference between probe and corresponding image position. From 240 sequences, standard deviation was under 5ms for standard imaging parameters. Source code is available in Public Library for Ultrasound Research, PLUS (www.plustoolkit.org).

Keywords: Tracked ultrasound, ultrasound calibration, temporal calibration, PLUS

1. Introduction

1.1. *Motivation*

Ultrasound (US) machines can be coupled with tracking systems that sample the probe's position and orientation (pose). Recorded poses are then associated with the corresponding US images, allowing each image to be positioned and oriented in 3-D space. However, the difference in hardware delays between the imaging and tracking systems produces a temporal offset that causes corresponding images and poses to receive different timestamps. To compensate for this misalignment temporal calibration is used to estimate the temporal offset between the image and tracker data.

1.2. *Prior work on temporal calibration*

Temporal calibration of US systems has been explored in a number of previous studies. Existing techniques can be divided into hardware-based and software-based techniques. Hardware-based techniques, for example [1], have a speed advantage compared to software-based techniques, but are generally inflexible; furthermore, many US systems are not be amenable to hardware modification. Software-based temporal calibration techniques can be roughly partitioned into those that use a volume reconstruction step and those that do not. In an attempt to limit the scope of this paper to a manageable size we restrict our attention to approaches that, like ours, do not involve a volume reconstruction step. It is, however, worth briefly mentioning that there are a number of existing volume reconstruction-based calibration techniques—see [2], for example. Volume reconstruction-based techniques have advantages, including the ability to implicitly account for changes in imaging parameters. There are, however, disadvantages: accurate spatial calibration is needed, the computational burden is increased, and all acquired frames must be stored, meaning that the volume cannot be reconstructed, in real-time, as it is being acquired.

Considering the calibration techniques that do not require volume reconstruction, we begin with Prager et al. [3,4], who perform temporal calibration by introducing a step perturbation into the image and tracker data through a sudden movement of the US probe. The image recording corresponding to the perturbation is automatically found by looking at the intensity difference between adjacent frames. The timestamp difference between the image and tracker recordings corresponding to the perturbation provides an estimate of the temporal offset. Although the simplicity of this approach is appealing, its accuracy is limited to the average of the tracker and image sampling periods. Furthermore, we have found that accurately detecting the perturbations in the image and tracker data can be difficult, causing the technique to be delicate in practice.

Addressing some of these deficiencies, Treece et al. [5] proposed a technique wherein a sequence of line motifs is introduced into the image data by imaging the bottom of a water tank with a probe undergoing an up-down motion. Next, the positions of the bottom of the water tank (derived from the line motifs) along with those of the probe (derived from the tracker data) are calculated. The temporal offset is then taken as the temporal shift that best aligns the image position and tracker position signals. Deriving the positions of the bottom of the water tank requires segmenting the line motif in each US image. To do this, they sample intensity information along regularly spaced vertical scan lines, compute the intersections between each scan line and the line motif, and then fit a line through the intersection points using the random sample consensus (RANSAC) algorithm [6]. To compute the intersection points, Treece et al. smooth and differentiate the intensity information along each scanline and then use the maximum of the derivative

signal. Their technique has improved accuracy when compared to that of Prager et al.. Treece et al.'s technique, however, appears to have some limitations in the image processing steps: smoothing the data set can distort the image and gradient information is sensitive to noise, which reduces the robustness of the techniques; furthermore, their algorithm has been reported to fail on noisy sequences [7]. The basic methodology presented by Treece et al. has been widely adopted [8,9,7]. Using a related approach, Rousseau et al. [7] proposed a fully-automatic temporal calibration algorithm, which, as in Treece et al., begins by producing a sequence of line motifs by imaging the bottom of a water tank. Next, the line motifs are segmented using the Hough transform and failed extractions are eliminated through continuity constraints on the detected lines. Lastly, the temporal offset is estimated by matching the extrema of the image position and the tracker position signals. When compared to Treece et al., the approach of Rousseau et al. has the advantage that the probe is not constrained to up-down motion. It has, however, two disadvantages. First, the extraction of line motifs using the Hough transform has a greater computational cost than the line-sampling RANSAC scheme. Second, alignment using only signal extrema, rather than the entire signal, discards a substantial amount of potentially useful information.

Along with the drawbacks already discussed, it should be noted that none of the above works provides a systematic validation of the algorithms over a range of imaging parameters. Additionally, the source code for the above algorithms is not readily available, making them challenging to use, reproduce, incorporate, or extend [10].

1.3. *Contribution*

In this work we present a correlation-based temporal calibration algorithm that, through a robust and fully automatic line detection scheme, improves on the work of Treece et al.. The algorithm is validated over a range of imaging parameters and all source code is freely available under a BSD license through the Public Library for Ultrasound research (PLUS) [11].

2. Methodology

We partition the temporal calibration process into four steps: (1) data acquisition, (2) construction of the image position signal, (3) construction of the tracker position signal, and (4) alignment of the image position and tracker position signals.

2.1. *Data acquisition*

We begin the calibration process by imaging a rubber sheet (approximately 2 cm thick) that is submerged in a water tank. It should be noted that the rubber sheet was used only as a means to increase the thickness of the wall of the tank being imaged; the choice of the rubber sheet was arbitrary and any material that produces a line motif should suffice. Under free-hand motion, we repeatedly move the probe towards and away from the rubber sheet while attempting to follow a purely translational and uniaxial trajectory. While deviations from a pure translational and uniaxial trajectory will slightly degrade the calibration, we have found that in practice any reasonably translational and uniaxial periodic free-hand motion is acceptable. For our experiments, the length of one period of probe motion was generally kept above 1 second, and the average length of collection was 47.2 seconds.

2.2. *Construction of the image position signal*

Signal construction begins by segmenting the line motif in each image. Segmentation is achieved by sampling intensity information along regularly spaced vertical scan lines (we used 40 sample lines per image), computing the intersections between each scan line and the line motif, and then fitting a line through the intersection points using the RANSAC algorithm (Figure 1). To find the intersection points we use a center-of-gravity (COG) approach (Figure 2).

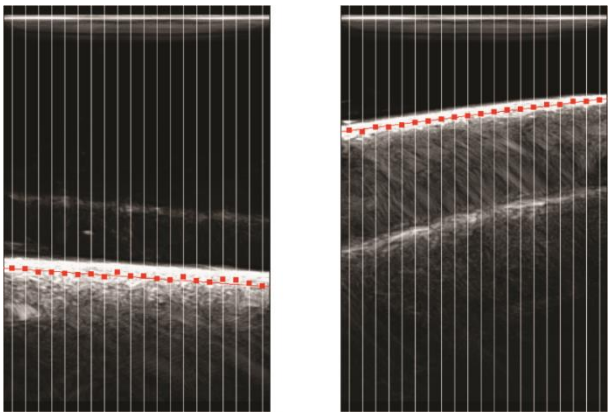

Fig. 1. Two average-quality ultrasound images with presence of secondary reflections; scanlines (white vertical lines), detected intensity peaks (red squares) and fitted lines (red lines)

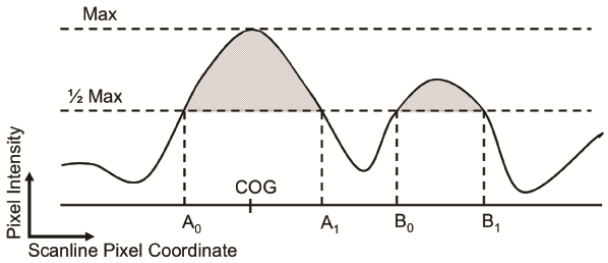

Fig. 2. Plot of pixel intensity vs. pixel coordinate along a sample scanline. There are two contiguous blocks of pixels above the threshold *1/2 Max:* $[A_0, A_1]$ and $[B_0, B_1]$. Because the intensity sum of $[A_0, A_1]$ is larger than that of $[B_0, B_1]$, $[A_0, A_1]$ is used to calculate the center-of-gravity (COG).

In the COG scheme we compute, for each scanline, the largest intensity sum along a contiguous block of pixels having intensities above half of the maximum intensity value along that scanline. Unlike the method by Treece *et al.*, the COG scheme does not use the gradient operator, which is sensitive to noise

and reduces robustness. To fit a line through the intersection points we used a generic implementation of the RANSAC algorithm by Yaniv [12], and left the parameters set to their default values. After computing the RANSAC line, the position of the image is taken as the detected line's *y* (vertical) coordinate at the image's *x* (horizontal) midpoint.

2.3. *Construction of the tracker position signal*

In forming the tracker position signal we ignore any rotational components of motion, leaving a sequence of position vectors that describe the probe's trajectory. To map the 3-D position vectors to scalar values, we compute, as in Treece *et al.*, the principal axis of probe motion using the principal component analysis (PCA) algorithm. The position vectors are then projected onto this principal axis. By projecting onto the principal axis of probe motion the algorithm is able to cope with probe motions that are not strictly uniaxial.

2.4. *Alignment of image and tracker positions*

In this step the tracker position and image position signals are aligned by minimizing the sum of squared differences (SSD) between the two signals (as in Treece et al.). To compute the SSD, the tracker position signal, which is generally denser than the video position signal, is resampled at the video position signal's timestamps via linear interpolation. Additionally, because the image and tracker positions are not of similar dimensions, the two signals are normalized by subtracting their means and dividing by their standard deviations.

Signal alignment proceeds in two phases. In the first phase, coarse alignment is achieved by minimizing the SSD of the tracker position and temporally shifted image position signals, where the temporal shifts are integer multiples of the average sampling period of the image data. In the second phase, alignment is improved with a finer (user-defined) temporal shift resolution. In our experiments, a 1 ms temporal shift resolution, which is the best timestamping accuracy that can be reliably achieved on standard PC hardware, was used for the second phase. An example of showing the unaligned and aligned position signals is shown in Figure 3.

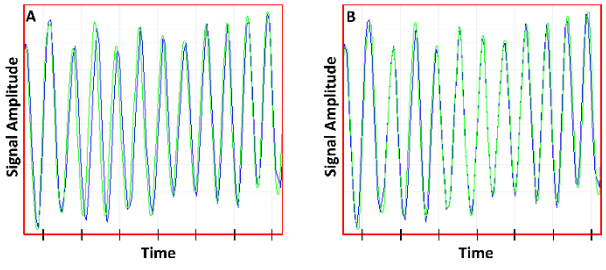

Fig. 3. (A) Unaligned and (B) aligned position signals. The blue curve corresponds to the image position signal and the green curve corresponds to the tracker position signal. The time between consecutive ticks on the time axis is 2 seconds. Signal amplitude has no unit, as it is a generic position signal normalized to the ±1.0 range.

2.5. *Software implementation*

The presented algorithm was implemented in C++ and is included in PLUS toolkit (www.plustoolkit.org), a free and open-source software package for real-time acquisition, processing, and broadcasting of medical imaging and tracking data. PLUS can get images directly through vendor-specific software interfaces from a number of US systems (such as Ultrasonix, Telemed, Interson, BK, and Philips) and indirectly, through framegrabbers, from other devices. PLUS provides fully automatic US probe spatial calibration, US image simulation, conversion, bone enhancement, and volume reconstruction algorithms. The toolkit can also collect data simultaneously from a wide range of other imaging and tracking devices and sensors, such inertial measurement units, spectrometers, and robotic devices that are useful for prototyping of new clinical interventional systems.

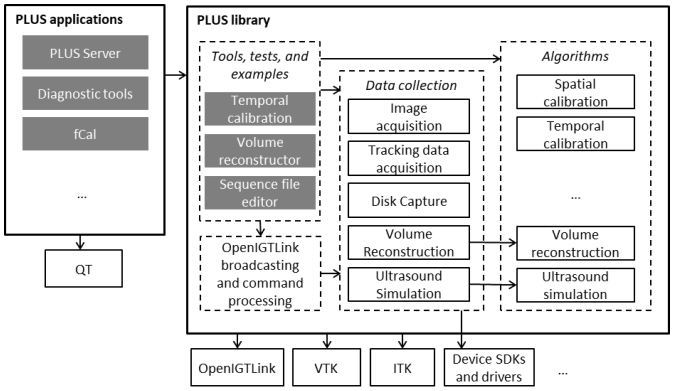

Fig. 4. PLUS toolkit architecture overview

Overview of PLUS architecture is show in Figure 4. The toolkit consists of a library component that contains all algorithms, device interfaces for data collection, and OpenIGTLink network communication. These are implemented based on open-source toolkits, such as VTK, ITK, OpenIGTLink, and they also use vendor-specific software development kits. PLUS library hosts a number of tools, tests and example applications, including a command-line tool for temporal calibration. PLUS applications contain additional tools and applications with convenient user interfaces, implemented using Qt framework.

2.6. *Experimental design*

To determine the algorithm's robustness and precision, and to investigate factors affecting the temporal offset, the algorithm was tested over a range of imaging parameters. In particular, we began the tests with a set of baseline imaging parameters and then proceeded to perturb the parameters, one at a time, from these baseline values. The baseline parameter set is listed in Table 1. All experiments were performed using the SonixTouch US system (Ultrasonix, Richmond, B.C., Canada) coupled with the SonixGPS electromagnetic (EM) pose tracking extension, allowing for simultaneous image acquisition and tracking. All

data was collected through the Ultrasonix research interface using the L14-5/38 Linear probe.

Table 1. Parameters for baseline study

Parameter	Value
Depth (cm)	5.5
Gain (dB)	25
Dynamic range (dB)	0
Focus points	5
Frequency (MHz)	6.6
Power	0
Frame rate	High (11 fps)
Map	4
Persist	0

3. Results

In total, 240 sequences were tested with no failed tests and an average computation time of 7.9 seconds per sequence (recall that the average sequence length was 47.2 seconds). The computed temporal offsets from the experiments are summarized in the following two sections. All acquired data are available upon request.

The mean temporal offset and corresponding standard deviation are listed in Table 2. Mean temporal offsets as a function of gain, depth, frequency, frame rate, persist, and focus are shown in Tables 3-8, respectively; corresponding standard deviations are also listed. Again, only one imaging parameter was varied at a time with the remaining parameters set to their baseline values (specified in Table 1).

Table 2. Baseline study

Tested sequences	Mean tracker lead (ms)
20	59.8 (± 3.0)

Table 3. Gain perturbations

Gain (dB)	Tested sequences	Mean tracker lead (ms)
35	10	60.5 (± 3.8)
45	10	62.6 (± 3.4)
55	10	63.1 (± 2.8)
65	10	64.2 (± 3.2)

Table 4. Depth perturbations

Depth (cm)	Tested sequences	Mean tracker lead (ms)
3.5	10	44.3 (± 2.9)
4.0	10	45.7 (± 4.4)
4.5	10	48.0 (± 4.1)
5.0	10	50.0 (± 1.8)
6.0	10	64.3 (± 3.6)
6.5	10	64.8 (± 2.5)
7.0	10	68.2 (± 3.4)

Table 5. Frequency perturbations

Frequency (MHz)	Tested sequences	Mean tracker lead (ms)
5.0	10	91.8 (± 10.8)
10.0	10	61.1 (± 1.4)

Table 6. Frame rate perturbations

Frame rate	Tested sequences	Mean tracker lead (ms)
Medium (9 fps)	10	74.3 (± 5.3)
Maximum (32 fps)	10	20.8 (± 3.4)

Table 7. Persists perturbations

Persist	Tested sequences	Mean tracker lead (ms)
2	10	55.8 (± 2.4)
4	10	55.2 (± 5.3)
6	10	159.1 (± 14.9)

Table 8. Focus perturbations

Number of focus points	Tested sequences	Mean tracker lead (ms)
6	10	71.1 (± 5.0)
7	10	89.3 (± 8.5)
8	10	110.9 (± 11.8)
9	10	126.3 (± 9.3)

4. Discussions

The COG line detection method properly functioned over all of the tested imaging parameters, a testament to its robustness. It is worth remarking that prior to adopting the COG approach we extracted lines using the Hough transform in a manner similar to that discussed in Rousseau et al.. We found, however, that the Hough transform was not well suited because the line motif usually appears as a thick band instead of a thin line. While the thick band could be reduced to a thin line through pre-processing steps, such as edge detection or thinning, such pre-processing discards much of the signal, can introduce artifacts and add additional complexity. There exist modified Hough transform algorithms that have been specifically adapted for thick line motifs, for example [13], but we did not pursue them, primarily because we felt that for a single line extraction the Hough transform approach was unnecessarily complicated.

In addition to the SSD metric, we tested two other alignment metrics: sum of absolute differences (SAD), and normalized cross-correlation. SAD was undesirable because it tended to produce correlation values that were relatively constant in the neighborhood of the optimal temporal offset—that is, flat shaped peaks on the SAD versus temporal offset plot. This characteristic made SAD alignment less reliable than alignment by cross correlation or SSD. Furthermore, through experimentation we found that in certain cases alignment using cross-correlation produced alignments that were visibly worse

than those produced with the SSD. For these reasons we opted to use SSD as the alignment metric.

From the results it is clear that changes in imaging parameters produced markedly different temporal offsets. For example, examining temporal offset as a function of imaging depth, the difference in temporal offset between a depth of 3.5 cm and a depth of 7 cm is nearly 25 ms. From tables 5-8, it is clear that similar, or more pronounced, variations in temporal offsets exist over perturbations in the frequency, frame rate, persist, and focus parameters. Because the variation is highly dependent on the implementation of the image processing chain of the specific ultrasound system, we will not discuss here the reasons for the changes in temporal offsets.

The range of temporal offsets suggests that different calibration parameters are needed for different US imaging parameters. A corollary of this is that a practical temporal calibration algorithm should be able to adequately function over a range of imaging parameters. We suggest performing temporal calibration under the range of US parameters to be used. If the variation in temporal offsets is determined to cause spatial errors exceeding those allowable for the given application, then appropriate steps can be taken to mitigate these errors. One mitigation strategy is to determine a maximum allowable hand motion speed and discard frames, and alert the user, when the hand motion speed exceeds this limit. Another solution is to store different temporal calibration offsets for different imaging parameters and vary which offset is used as the imaging parameters are varied. Alternatively, in settings where imaging parameters are frequently tuned, volume reconstruction-based calibration techniques may be useful because, as mentioned previously, adaptation to parameter changes is implicit.

We also examined how the temporal offset does depend on the imaging parameters, on machine of different vendors. We performed 10 temporal calibrations with the same Ascension TrackStar EM tracker, sensors, and computer with both Ultrasonix and Telemed ultrasound. The time offsets were slightly different at a depth of 50 mm, for Ultrasonix it was 50 +/- 1.8 ms and for Telemed 32 +/- 1.9 ms. We note that the delay of the imaging system is dependent on many parameters in the image processing pipeline, and some of the image processing parameters are not accessible for the user to set. Therefore, different ultrasound machines take a different amount of time to process the same image from the raw signal of the ultrasound transducer to the B-mode ultrasound image. In addition, Tables 2-8 show how the temporal offset depends on the imaging parameters for a given ultrasound machine.

To examine how probe orientation affects the results, we ran 10 calibration sequences with an Ultrasonix linear transducer at a focal depth of 50 mm, in each orientation of +30, 0, -30 degrees. The change in the temporal offset results was negligible, consistently less than 0.1 ms. The explanation is that a tilt angle may make some noticeable difference if there is a large and variable beam width. But if the bottom of the flat water tank is kept around the focus point of the image, then a tilted orientation should make no difference in the temporal calibration, just as our experiment showed.

A notable feature of this work is that all source code is available under a BSD license as part of PLUS; the code is freely usable for any purpose, without any limitation, even commercially. By including our work as a part of PLUS, we hope to not only facilitate the usage of our algorithm with other tracked US functionalities, but also to promote extension and/or modification of our work to suit custom applications. PLUS also generalizes the presented algorithm by allowing it to be used for temporal calibration of any number of imaging and tracking devices (e.g., temporal calibration of optical tracker data, electromagnetic tracker data, and US data) by pairwise computation of the temporal offset; PLUS also allows the temporal calibration of arbitrary tracking devices, including those not related to US systems. Combined, these factors greatly increase the practicality of our work.

The ease-of-use, extensibility, and effectiveness of our temporal calibration are attested to by its usage on devices by many groups on a variety of devices, including the Ultrasonix, BK, Hitachi, and Fraunhofer DiPhAS ultrasound systems (through research interface, framegrabber, and OpenIGTLink interfaces), the Ascension trakSTAR, and NDI Aurora electromagnetic trackers, and the Claron MicronTracker, and NDI Polaris optical trackers (see, for example, [14-20]).

Finally, regarding whether a "ground truth" is available, we note that the exact value of temporal offset depends on the both hardware and software of the ultrasound machine and transducer and the position tracker and sensors used. Keeping these the same but with using different constrained motion patterns one should receive the same temporal offset. Still, this still would not be "ground truth", only a somewhat different way to estimate the temporal offset. Our approach of uniaxial motion in a flat water tank at the image's focal depth is perhaps the simplest and most robust way to measure the temporal offset. A more complex constrained motion pattern would be subject to potential errors in enforcing the constraints and in processing the ultrasound images. Instead, we are content with the high level of consistency and precision indicated by low standard deviations found throughout our experiments.

5. Conclusions

This work presents a temporal calibration algorithm equipped with a robust line detection scheme. The precision of the algorithm was systematically evaluated over a range of imaging parameters, with normal imaging parameters resulting in standard deviations under 5 ms and extreme imaging parameters resulting in standard deviations up to 15 ms. By providing the algorithm as part of the Public Library for Ultrasound research (PLUS) this work aims to make a practical contribution to ultrasound research.

Acknowledgments

Gabor Fichtinger is supported as a Cancer Care Ontario Research Chair in Cancer Imaging. This work was co-funded as an Applied Cancer Research Unit of Cancer Care Ontario with funds provided by the Ontario Ministry of Health and Long-Term Care. This work has been partially supported by the

United States National Institutes of Health through the grant entitled SLICER+PLUS: collaborative, open-source software for ultrasound analysis (1 R01 EB021396-01A1).

References

[1] Boctor EM, Choti MA, Burdette EC, Webster RJ (2008) Three-dimensional ultrasound-guided robotic needle placement: an experimental evaluation. The International Journal of Medical Robotics + Computer Assisted Surgery: MRCAS 4 (2):180-191. doi:10.1002/rcs.184

[2] Gooding MJ, Kennedy SH, Noble JA (2005) Temporal calibration of freehand three-dimensional ultrasound using image alignment. Ultrasound in Medicine and Biology 31 (7):919-927. doi:10.1016/j.ultrasmedbio.2005.04.007

[3] Prager RW, Gee A, Berman L (1999) Stradx: real-time acquisition and visualization of freehand three-dimensional ultrasound. Medical Image Analysis 3 (2):129-140. doi:10.1016/s1361-8415(99)80003-6

[4] Meairs S, Beyer J, Hennerici M (2000) Reconstruction and visualization of irregularly sampled three- and four-dimensional ultrasound data for cerebrovascular applications. Ultrasound in Medicine and Biology 26 (2):263-272. doi:10.1016/s0301-5629(99)00130-1

[5] Treece GM, Gee AH, Prager RW, Cash CJC, Berman LH (2003) High-definition freehand 3-D ultrasound. Ultrasound in Medicine and Biology 29 (4):529-546. doi:10.1016/s0301-5629(02)00735-4

[6] Fischler MA, Bolles RC (1981) Random sample consensus: a paradigm for model fitting with applications to image analysis and automated cartography. Communications of the ACM 24 (6):381-395. doi:10.1145/358669.358692

[7] Rousseau F, Hellier P, Barillot C (2006) A novel temporal calibration method for 3-D ultrasound. Medical Imaging, IEEE Transactions on 25 (8):1108-1112. doi:10.1109/tmi.2006.877097

[8] Khamene A, Sauer F (2005) A Novel Phantom-Less Spatial and Temporal Ultrasound Calibration Method. In: Duncan J, Gerig G (eds) Medical Image Computing and Computer-Assisted Intervention – MICCAI 2005, vol 3750. Lecture Notes in Computer Science. Springer Berlin Heidelberg, pp 65-72. doi:10.1007/11566489_9

[9] Mercier L, Del Maestro R, Petrecca K, Kochanowska A, Drouin S, Yan CB, Janke A, Chen S-S, Collins DL (2011) New prototype neuronavigation system based on preoperative imaging and intraoperative freehand ultrasound: system description and validation. Int J CARS 6 (4):507-522. doi:10.1007/s11548-010-0535-3

[10] Ince DC, Hatton L, Graham-Cumming J (2012) The case for open computer programs. Nature 482 (7386):485-488

[11] Lasso A, Heffter T, Rankin A, Pinter C, Ungi T, Fichtinger G (2014) PLUS: Open-Source Toolkit for Ultrasound-Guided Intervention Systems. Biomedical Engineering, IEEE Transactions on 61 (10):2527-2537. doi:10.1109/tbme.2014.2322864

[12] Yaniv Z (2010) Random sample consensus (RANSAC) algorithm, a generic implementation. Insight Journal

[13] Lo R, Tsai W (1995) Gray-scale hough transform for thick line detection in gray-scale images. Pattern Recognition 28 (5):647-661. doi:10.1016/0031-3203(94)00127-8

[14] Al-Deen Ashab H, Lessoway VA, Khallaghi S, Cheng A, Rohling R, Abolmaesumi P (2013) An Augmented Reality System for Epidural Anesthesia (AREA): Prepuncture Identification of Vertebrae. Biomedical Engineering, IEEE Transactions on 60 (9):2636-2644. doi:10.1109/tbme.2013.2262279

[15] Jansen N, Brennecke T, Hirschfeld J, Colter L, Raczkowsky J, Woern H, Schipper J Rotatable flexible neck-model for the evaluation of minimally invasive operation procedures with the help of an ultrasound-based navigation system. In: Engineering in Medicine and Biology Society (EMBC), 2013 35th Annual International Conference of the IEEE, 3-7 July 2013 2013. pp 1140-1143. doi:10.1109/embc.2013.6609707

[16] Shah A, Zettinig O, Maurer T, Precup C, Schulte zu Berge C, Weiss J, Frisch B, Navab N (2014) An Open Source Multimodal Image-Guided Prostate Biopsy Framework. In: Linguraru MG, Oyarzun LC, Shekhar R, Wesarg S, González BMA, Drechsler K, Sato Y, Erdt M (eds) Clinical Image-Based Procedures. Translational Research in Medical Imaging, vol 8680. Lecture Notes in Computer Science. Springer International Publishing, pp 1-8. doi:10.1007/978-3-319-13909-8_1

[17] Wang J, Shivaprabhu V, Galeotti J, Horvath S, Gorantla V, Stetten G (2014) Towards Video Guidance for Ultrasound, Using a Prior High-Resolution 3D Surface Map of the External Anatomy. In: Linte C, Yaniv Z, Fallavollita P, Abolmaesumi P, Holmes D, III (eds) Augmented Environments for Computer-Assisted Interventions, vol 8678. Lecture Notes in Computer Science. Springer International Publishing, pp 51-59. doi:10.1007/978-3-319-10437-9_6

[18] Paniagua B, Zukic D, Ortiz R, Aylward S, Golden B, Nguyen T, Enquobahrie A (2015) Ultrasound-Guided Navigation System for Orthognathic Surgery. In: Linte CA, Yaniv Z, Fallavollita P (eds) Augmented Environments for Computer-Assisted Interventions, vol 9365. Lecture Notes in Computer Science. Springer International Publishing, pp 1-10. doi:10.1007/978-3-319-24601-7_1

[19] Klemm M, Kirchner T, Gröhl J, Cheray D, Nolden M, Seitel A, Hoppe H, Maier-Hein L, Franz AM (2016) MITK-OpenIGTLink for combining open-source toolkits in real-time computer-assisted interventions. Int J CARS, 1-11, doi:10.1007/s11548-016-1488-y

[20] Nijkamp J, Schermers B, Schmitz S, de Jonge S, Kuhlmann K, van der Heijden F, Sonke JJ, Ruers T (2016) Comparing position and orientation accuracy of different electromagnetic sensors for tracking during interventions, Int J CARS, 11 (8):1487-1498

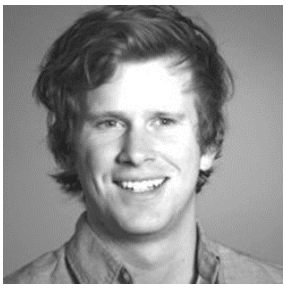

Eric Moult received his bachelor's degree in electrical engineering from Queen's University, Canada, with first class honours. He is currently a doctoral candidate in medical engineering and medical physics in the Harvard-MIT Health Sciences and Technology Program (Cambridge, MA, USA). His research focus on using engineering and computer science techniques to solve problems in medical imaging.

Andras Lasso (M'09) received the doctoral degree in computer science from the Technical University of Budapest, Budapest, Hungary, in 2011. He is currently a senior research engineer in the School of Computing at Queen's University, Canada, where he is the associate director of engineering of the Percutaneous Surgery Laboratory. His main interests are developing high-quality, reusable, open-source software components and using them to build systems for translational research and clinical use.

Tamas Ungi Tamas Ungi received medical doctor degree in 2006 and PhD in 2010 from the University of Szeged, Hungary. He is currently a senior research scientist and adjunct assistant professor at the School of Computing and at the Department of Surgery at Queen's University, Canada. His research focus is clinical translation of imaging and navigation technology in surgical, radiological, and medical education applications. He is a regular contributor to the source code and tutorials of the open-source SlicerIGT platform that facilitates quick prototyping of translational clinical research applications.

Csaba Pinter Csaba Pinter received the BSc and MSc degrees in informatics from the University of Szeged, Hungary. Having spent several years in the medical imaging software industry, currently he is a research software engineer at the School of Computing, Queen's University, Canada. His work concentrates on open source software platforms for medical image analysis and image-guided therapies. He is an active contributor to 3D Slicer and he is the principal developer of the SlicerRT toolkit for radiation therapy.

Mattea Welch received her bachelor's degree in biomedical computing from Queen's University, Canada, with honours. She is currently a doctoral candidate in the medical biophysics program at the Faculty of Medicine, University of Toronto. Her research focuses on developing novel pattern recognition techniques for predictive models for the diagnosis and treatment of cancer.

Gabor Fichtinger (M'04, S'2012, F'2016) received the doctoral degree in computer science from the Technical University of Budapest, Budapest, Hungary, in 1990. He is a Professor in the School of Computing, with cross appointments in the departments of Mechanical and Material Engineering, Electrical and Computer Engineering, Surgery and Pathology at Queen's University, Canada, where he directs the Percutaneous Surgery Laboratory. His research specializes on medical imaging and computer-assisted interventions, primarily for cancer diagnosis and therapy. He holds a Cancer Care Ontario Research Chair in Cancer Imaging.